Journal of Materials Science Research and Reviews

Volume 7, Issue 4, Page 551-565, 2024; Article no.JMSRR.123352

Tailoring Graphene for Enhanced Biosensing: Structural Modifications and Modeling of Electronic and Optical Properties

Samwel Onyango Okoth [a], Godfrey Okumu Barasa [a*], John Onyango Agumba [a], Antonate Wanyonyi [a] and Edwin Atego [a]

[a] Department of Physical Sciences, Jaramogi Oginga Odinga University of Science and Technology, P.O Box 210-40601, Bondo, Kenya.

Authors' contributions

This work was carried out in collaboration among all authors. All authors read and approved the final manuscript.

Article Information

Open Peer Review History:
This journal follows the Advanced Open Peer Review policy. Identity of the Reviewers, Editor(s) and additional Reviewers, peer review comments, different versions of the manuscript, comments of the editors, etc are available here: https://www.sdiarticle5.com/review-history/123352

Original Research Article

Received: 14/07/2024
Accepted: 17/09/2024
Published: 25/09/2024

ABSTRACT

The main objective of this study was to investigate the impacts of structural modifications on the electronic and optical properties of graphene to improve its biosensing capabilities. The remarkable optical and electrical properties of two-dimensional graphene were found to make it highly promising for use in a wide range of technological applications. However, the absence of a band gap in pure graphene has been identified as a limitation for its use in critical applications such as biosensing. To address this, modeling and simulation approaches were employed for structural

**Corresponding author: Email: gobarasa@jooust.ac.ke, gobarasa@yahoo.com;*

Cite as: *Okoth, Samwel Onyango, Godfrey Okumu Barasa, John Onyango Agumba, Antonate Wanyonyi, and Edwin Atego. 2024. "Tailoring Graphene for Enhanced Biosensing: Structural Modifications and Modeling of Electronic and Optical Properties". Journal of Materials Science Research and Reviews 7 (4):551-65. https://journaljmsrr.com/index.php/JMSRR/article/view/349.*

alterations using the Material Studio 7.0 CASTEP module. The electronic and optical properties of monolayer and bilayer graphene crystals, including doped and defective forms, were examined. Doping with phosphorus and aluminum was found to induce band gaps of 0.0147 eV and 0.0103 eV, respectively, while vacancies significantly altered the density of states. A band gap energy of 0.110 eV was observed in bilayer graphene, signifying a transition from a metallic or semi-metallic state to a semiconductor state. This energy range corresponds to the infrared region of the electromagnetic spectrum, suggesting that bilayer graphene with such a band gap could be useful for devices like infrared detectors and sensors. The greatest peak energy of 11.4 eV was observed in monolayer graphene with vacancy, which is higher than that of its pure and doped counterparts, indicating the presence of electronic states in the conduction band region. The defect-induced generation of electronic states within the band structure was responsible for the significant increase in the density of states, with a DOS value of 47.3 electrons per eV. Refractive indices ranging from 1.45 to 3.47 were recorded, with bilayer graphene showing a higher refractive index of 3.06, indicating greater light absorption and reduced transparency. The absorption coefficient characteristics of vacancy-containing bilayer structures were found to differ from those of monolayer structures. Moreover, dielectric function analysis revealed a stronger imaginary peak of approximately 40 for bilayer graphene with vacancy, followed by the bilayer structure with a peak of 15, indicating increased light absorption due to the introduction of vacancies and additional layers. In the conductivity analysis of bilayer graphene, the highest imaginary peak at 17 eV was identified as the wavelength where graphene absorbed light most effectively. For biosensing systems relying on light-matter interactions, this peak represents the energy required for electronic transitions within the material. In conclusion, the findings demonstrate the potential of specially tailored graphene-based biosensors with enhanced sensitivity and specificity, which could be applied in biological and environmental monitoring, paving the way for highly efficient sensing platforms.

Keywords: Biosensors; doping; optical; electrical; selectivity and sensitivity.

1. INTRODUCTION

Graphene's large surface area [1], enhanced electrical conductivity [2], and biocompatibility [3] make it an excellent material for biosensing applications. When used into biosensors, graphene offers potential for extremely sensitive [4], selective [5], and quick detection [6] platforms for a variety of biomolecules. The full promise of graphene-based biosensors cannot be realized until obstacles such as improving bio-recognition, ensuring stability under physiological settings, and increasing sensitivity are addressed [7]. In recent years, major efforts have been made to boost the performance of graphene-based biosensors via nanoscale structural alterations. These modifications, which vary from hybrid nanostructure engineering [8] to biomolecule functionalization [9], are intended to enhance both sensing capability and the interface between biological recognition elements and graphene. Recent studies assert that there has been substantial advancement in this field of study. For instance, research has demonstrated that functionalizing graphene with certain biomolecules, like DNA probes [10] or antibodies, can greatly improve the selectivity and specificity of the biosensor. Moreover, it has been discovered that combining graphene's properties with those of other nanomaterials [11], such as carbon nanotubes or metal nanoparticles, may improve signal amplification and sensitivity [11,12]. Adding defects or nanopores is one of the innovative morphological modifications that researchers have looked into to enhance graphene's electrical properties and biomolecular interactions [13]. The developments show the continuous efforts to get above the challenges and achieve full potential of biosensing technology derived from graphene. Higher-level discoveries have also been made in various disciplines as a result of the diverse features of graphene and other carbon-based materials [14]. In order to solve the issues given by the semi-metallic property of graphene and the substantial cost of its synthesis, scientists investigated into structural changes such doping [15,16,17] and defect engineering [18]. For a variety of applications, studying and enhancing graphene's characteristics can be accomplished through modeling and simulation. The goal of other recent initiatives has likewise been to improve the performance of graphene-based biosensors by nanoscale structural alterations. Despite this, many uncertainties remain regarding how these modifications may impact biological recognition elements [19,20,21]. The goal of this research is to close the information gaps and offer fresh

perspectives on how structural alterations impact the optical, electrical, and biosensing characteristics of graphene crystals [22, 23]. Our primary objective is to simulate novel structures and thoroughly examine the effects of structural alterations, such as dopants, vacancies, and layers, on optical and electrical properties. This work provides a new perspective on exploiting graphene's promise for biosensing applications by closely examining many structural changes and their direct implications on biosensing performance.

2. METHODOLOGY

A new project was created in Material Studio and named accordingly. To import a graphite structure, we proceeded as follows; File> Import> Structures > Ceramics > Graphite. A model of Graphite structure was obtained. We started by building a graphite framework in order to develop the graphene structure. After that, the transformation was carried out into graphene using a number of methodical procedures. To establish the first symmetry, we first navigated to the task bar and picked 'Build,' followed by 'Symmetry,' and then 'Make P1' [24]. Then, we eliminated a layer from the structure by selecting it, doing a right-click, and then removing it. In this stage, the transformation of graphite into graphene—a single layer of graphite—was ensured. Henceforth, we employ the 'Find Symmetry' function found under 'Build' > 'Symmetry' to locate and apply the suitable symmetry to the framework. Utilizing the 'Super Cell' function with dimensions set at 2×2×2, we reproduced the unit cell in accordance with the expansion of the graphene lattice [25]. This process preserves the essential characteristics of graphene while enabling the formation of a bigger lattice. In addition, we used the 'Rebuild crystal' tool found under 'Build' > 'Crystals' > 'Rebuild crystal,' where we entered particular lattice parameters, to guarantee precise depiction. In this case, the lattice parameters are defined as follows: α = 90, β = 90, γ = 120, a = 2.459756, b = 2.459756, c = 25.000000. These factors control the lattice's geometric properties, which are essential for the creation of graphene. Lastly, we used the 'Super Cell' tool again, adjusting the dimensions to 5×5×1, to obtain the appropriate dimensions and complete the graphene model. This step led to the formation of a monolayer graphene structure. By carefully carrying out these procedures, we guarantee the precise creation of a graphene model that complies with accepted crystallographic and symmetry operations principles and is supported by science.

In order to begin the process of creating a bilayer graphene sheet, we first created a new folder called "graphene bilayer" inside of the same newly formed Material Studio project. We repeated the procedure to produce a monolayer graphene structure as described earlier with all the parameters satisfied. We next added another layer to obtain the bilayer graphene structure. This was done as follows, go to 'Build' > 'Build Layers' > 'Add layer 1 and 2 of monolayer,' making sure that a bilayer structure is created. Lastly, we choose 'Check create layered structure as a crystal' and execute the 'create' command to verify the creation of the bilayer graphene crystal. When all is said and done, the resulting crystal structure was a bilayer of graphene. We guarantee the accurate production of a bilayer graphene model in the Material Studio environment by adhering to these rigorous steps. From the bilayer graphene structure, we created a vacancy by following rigorous steps of creating a bilayer graphene structure on a newly created file named bilayer with vacancy. Two carbon atoms were selected from the bilayer graphene and deleted. The new structure with two atoms was resulted named bilayer graphene with vacancy [26,27,28]. Following similar procedure of creating a graphene monolayer, a new graphene monolayer structure was created. One atom was then selected and deleted to create a vacancy, this resulted to a new structure of monolayer graphene with vacancy. Further structures were created by doping with Aluminium and Phosphorous as follow; the two monolayer graphene was created separately and named with respective dopants. On each structure five carbon atoms was selected, Aluminium was substituted with the selected carbon atoms to form a new structure called monolayer graphene doped with Aluminium. A further substitution of carbon atoms with Phosphorous on the other structure resulted to monolayer graphene doped with Phosphorous.

2.1 Computational Methods

The electronic and optical characteristics of the graphene sheet were ascertained using the Density Functional Theory(DFT) calculation. DFT calculations was chosen because it offers a realistic, accurate, and adaptable framework for researching the structural and electronic properties of materials while still being computationally possible. Further DFT is the

method of choice for material science, chemistry, and physics research because of its broad modeling capability, robust software support, and ability to balance computational cost and accuracy. The CASTEP technique and OTFG(On-The-Fly Generated) ultrasoft pseudopotentials was used for all computations. Ultrasoft pseudopotentials were used to simplify the complex interactions between valence electrons and the ion core in a material, allowing for more efficient simulations of electronic structures while maintaining accuracy. The OTFG approach allowed for greater flexibility and precision in tailoring the pseudopotential to specific conditions in real-time, which is particularly useful in materials science simulations. We computed the exchange correlation energy in the generalized gradient approximation (GGA) using the Perdew-Burke-Ernzerhof (PBE) functional. A plane-wave energy cutoff of 326.5 eV was used for all calculations. This cutoff was maintained throughout. In order to maximize the geometry of graphene sheets, a 1×2×1 with relativistic Koelling-Harmony treatment was be used to sample the k-point of the Brillouin zone. The energy convergence tolerance for all structural relaxations set to 2×10^{-6} eV/atom during geometry optimizations. With a maximum stress of 0.1 GPa, the self-consistent field convergence tolerance (SCF) was set to 2×10^{-6} eV/atom. The CASTEP module was used to simulate the graphene-modeled structures in order to achieve the required properties.The graphene structure was embedded in a unit cell of parameters; a = 2.459756, b = 2.459756, c =25.000000 having cell angles of alpha =90, beta = 90 and gamma = 120. The Brillouin zone path was set at

$$\mathrm{G}(0.000, 0.000, 0.000) \rightarrow A(0.000,\ 0.000,\ 0.500) \rightarrow H(-0.333, 0.667, 0.500) \rightarrow K(-0.333, 0.667, 0.000) \rightarrow \mathrm{G}(0.000, 0.000, 0.000)\ .$$

3. RESULTS AND DISCUSSION

3.1 Electronic Band Properties

The Fig. 1(a-b) shows band structures of monolayer and bilayer graphene obtained after simulation and analysis. From the band structure graphs, we were able to obtain band gap energy in eV as shown in Table 1.

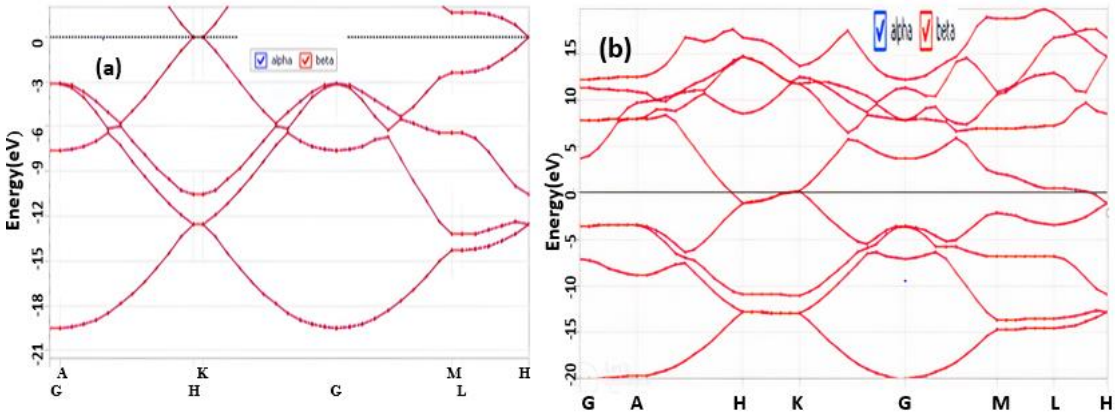

Fig. 1. (a) Band structure of Monolayer and (b) Bilayer

Table 1. The band gap energies for different graphene structures, such as variously doped or bilayer topologies and pure monolayer graphene; comparison between calculated values and values obtained from other previously reported works

Structures	Band gap in eV (calculated values)	Experimental values of Band gap from other previously reported works
Mono-layer graphene	0.000	0.000 [20]
Mono-layer doped with Phosphorous	0.0147	0.030[21]
Mono-layer doped with Aluminium	0.0103	0.012[22]
Mono-layer with Vacancy	0.0197	0.023 [23]
Bi-layer Graphene	0.110	0.250[24]
Bi-layer with Vacancy	0.356	0.400[25]

The band gap energies for different graphene structures, such as pure monolayer graphene and various doped or bilayer forms, are shown in Table 1. These values are important markers of graphene's optoelectronic characteristics, which are important for biosensing applications [29]. First of all, the calculated values shows that pure monolayer graphene has a zero band gap that is consistent with other scholarly works for example Castro and co-workers (2009), which is in line with its behavior as a semimetal. Although according to Zhang *et al.,* this feature renders it very conductive, the difficulties of attaining high sensitivity and selectivity limit its application in biosensing [30]. The band gap of graphene can be altered, though, by adding dopants or defects like vacancies, aluminum (Al) or phosphorous (P) doping, or creating bilayer structures. This opens up new possibilities for biosensing. Potential gains in the sensitivity and selectivity of graphene-based biosensors are indicated by the small band gap values for doped graphene structures (0.0147 eV for Phosphorous doped and 0.0103 eV for Aluminium doped), which indicate successful doping effects. The band gap values reported are attributed to the introduction of additional energy levels in the band structure via phosphorous and aluminum doping [31]. Moreover, the electronic characteristics of graphene are influenced by the existence of vacancies (0.0197 eV for monolayer with vacancy), which leads to a finite band gap. This implies that vacancies change graphene's electrical structure and affect how well-suited it is for biosensing uses. It's interesting to note that, in comparison to monolayer graphene, the band gap rises dramatically in bilayer graphene arrangements, reaching values of 0.110 eV for bilayer graphene; this values is in close agreement with *Zhang et al.* (2009) which reported 0.250 eV and 0.356 eV for bilayer with vacancy graphene. This finding is in agreement with twisted double-bilayer graphene [32]. In bilayer graphene, a band gap of 0.110 eV signifies a change from a metallic or semi-metallic state to a semiconducting state. This value not only implies that the band gap can be tuned, which opens up new possibilities for applications in optoelectronics and nanoelectronics, but it also correlates to an energy range in the infrared region of the electromagnetic spectrum. Thus, infrared detectors, sensors, and other optoelectronic devices could make good use of bilayer graphene with such a band gap. The inclusion of an additional graphene layer or vacancies between the layers altered the electrical structure, leading to interlayer interactions and an increase in the Graphene's band gap [33-34] can be tuned by bilayer topologies, vacancies, or doping, which can improve the sensitivity, selectivity, and detection limits of graphene-based biosensors. Furthermore, comprehending the connection between band gap and electronic characteristics offers important new perspectives for developing and refining graphene-based biosensing systems [35] that are customized for certain analytes and uses [36]. All things considered, the findings shown in Table 1, highlight how crucial band gap engineering in graphene is to the advancement of biosensing technology band gap. Furthermore, these results have important ramifications for biosensing applications.

After analysis various density of states for all the graphene modeled structures were displayed and Fig. 2 (a-b) are such sampled figures representing density of states for bilayer with vacancy and monolayer doped with Aluminium. These graphs provide the highest peak energy and their corresponding density of state values as the y-axis parameter and Table 2 compiles these values and subsequent discussion follows.

The density of state (DOS) results that are displayed in Table 2 provide important knowledge regarding the distribution of electronic states within the material's energy spectrum. Each entry in the table corresponds to a particular graphene configuration and details the highest peak energy (in eV) and the DOS (in electrons per eV). These results shed light on the potential for biosensing applications of the various graphene structures that were investigated in our study. To begin with, monolayer graphene configurations showed that there are electronic states present, mainly centered on the Fermi level, with the maximum peak energy of -8.00 eV for pure monolayer graphene. A linear dispersion relation close to the Dirac point characterizes the material's intrinsic features, which are consistent with the very low density of states indicated by the DOS value of 1.61 electrons per eV. But after doping with aluminum or phosphorous, notable changes are seen in the maximum peak energy and DOS. Phosphorous-doped monolayer graphene has a significantly higher DOS value of 18 electrons per eV along with a higher peak energy of -7.10 eV. Likewise, Aluminium-doped monolayer graphene exhibits a significant rise in DOS to 14.9 electrons per eV along with a shift in the

greatest peak energy to -5.87 eV. Peak energy and DOS changes demonstrate how dopants affect the electronic structure of the material, bringing to the development of localized electronic states and increased charge carrier density. Further, the DOS properties of monolayer graphene undergo significant alterations upon the vacancy introduction. The greatest peak energy of monolayer graphene with vacancy is 11.4 eV, which is much greater than that of its pure and doped equivalents and suggests the existence of electronic states in the conduction band area. The generation of defect-induced electronic states within the band structure is responsible for the significant rise in the density of states, as indicated by the DOS value of 47.3 electrons per eV. Going on to bilayer graphene structures, the DOS properties show variations from their monolayer equivalents. When compared to monolayer graphene, bilayer graphene exhibits a slightly shifted peak energy of 8.6 eV and a similar DOS value of 1.52 electrons per eV. This implies that interlayer interactions affect the distribution of electronic states in bilayer graphene, resulting in minute differences in DOS properties, even while the material has a comparable overall electronic structure. Lastly, the addition of vacancies to bilayer graphene led to additional changes in DOS parameters. When compared to pristine bilayer graphene, bilayer graphene with vacancy has a higher peak energy of 9.23 eV and a higher DOS value of 16.5 electrons per eV. These alterations indicate that defects have an impact on bilayer graphene's electrical characteristics, resulting in the creation of new electronic states within the band structure. In general, the DOS results offer thorough understandings of the electrical characteristics of the graphene-based structures examined in this work. Peak energy and DOS characteristics show how dopants and defects affect the electronic structure of the material; this information is useful for optimizing graphene-based biosensors with improved sensitivity and selectivity for environmental and biomedical sensing applications [37].

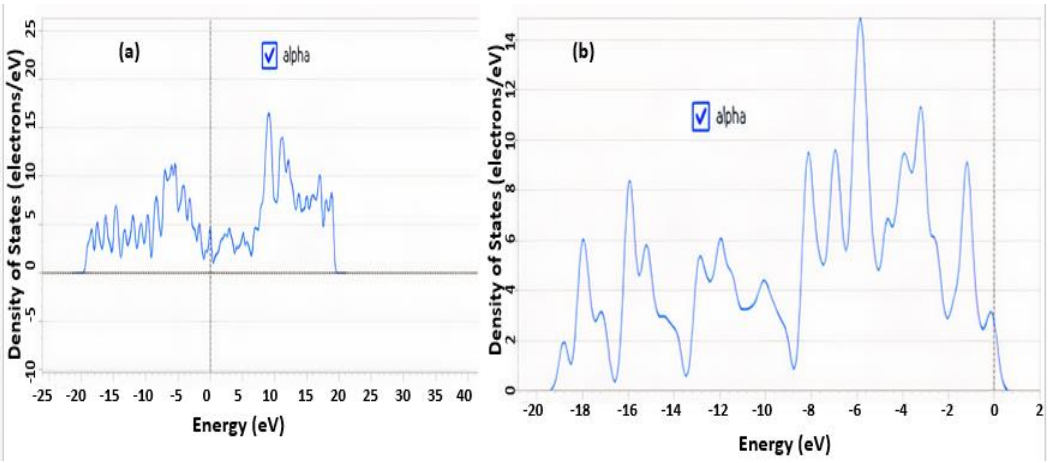

Fig. 2. (a) Density of State of Bilayer with Vacancy and, (b) Monolayer doped with Aluminium

Table 2. Graphene configuration and details of the highest peak energy (in eV) and the DOS (electrons/eV) for both calculated and previously reported values from other works.

Structures	Highest peak energy (eV) (Calculated values)	Values from other previously reported works	DOS (electrons/eV)	DOS Values from other previously reported works
Mono-layer graphene	-8.00	-7.5[34]	1.61	2.0[34]
Mono-layer doped with Phosphorous	-7.10	-7.2 [21]	18	19[21]
Mono-layer doped with Aluminium	-5.87	-6.0 [22]	14.9	15[22]
Mono-layer with vacancy	11.4	12.0[23]	47.3	50[23]
Bi-layer	8.6	9.0[24]	1.52	1.5[24]
Bi-layer with vacancy	9.23	9.5[25]	16.5	17[25]

3.2 Optical Properties

3.2.1 Refractive index

Li and coworkers, previous had found that in the visible spectrum, pure graphene usually has a refractive index of about 1.0 [38], suggesting almost complete transparency. Refractive index can go up a little when doped or altered, but it still stays low when compared to many other materials used in biosensors. This characteristic of graphene reduces signal loss and allows for sensitive detection by facilitating effective light transmission through the sensor [39]. The refractive index can be calculated from graphs by directly reading off the real and imaginary components of the refractive index or using related optical properties (e.g., dielectric function or absorption coefficient) through a mathematical relations in equation 1; $\tilde{n} = n + ik$. The refractive index $\tilde{n}$ is generally a complex, the real part n determines the phase velocity of light, and the imaginary part k describes how much light is absorbed as it travels through the material. The Fig. 3 a-b are some of the indices graphs that were obtained, from these graphs refractive index of each structure was directly read and compiled in Table 3.

The refractive index values found for different graphene configurations offer important information about their optical characteristics, which may influence how biosensors might use them. With a refractive index of 1.45, pristine monolayer graphene is very transparent and appropriate for biosensing applications that is needed for effective light transmission [40]. On the other hand, adding vacancy to monolayer graphene raises the refractive index to 1.59, which change how light interacts with matter and have an effect on sensitivity. Phosphorus (1.31) or aluminum (1.58) doping of monolayer graphene changes its optical and electrical structure, providing tunability for customized biosensor designs. In contrast to monolayer graphene, bilayer graphene exhibits a higher refractive index of 3.06, indicating greater light absorption and decreased transparency.

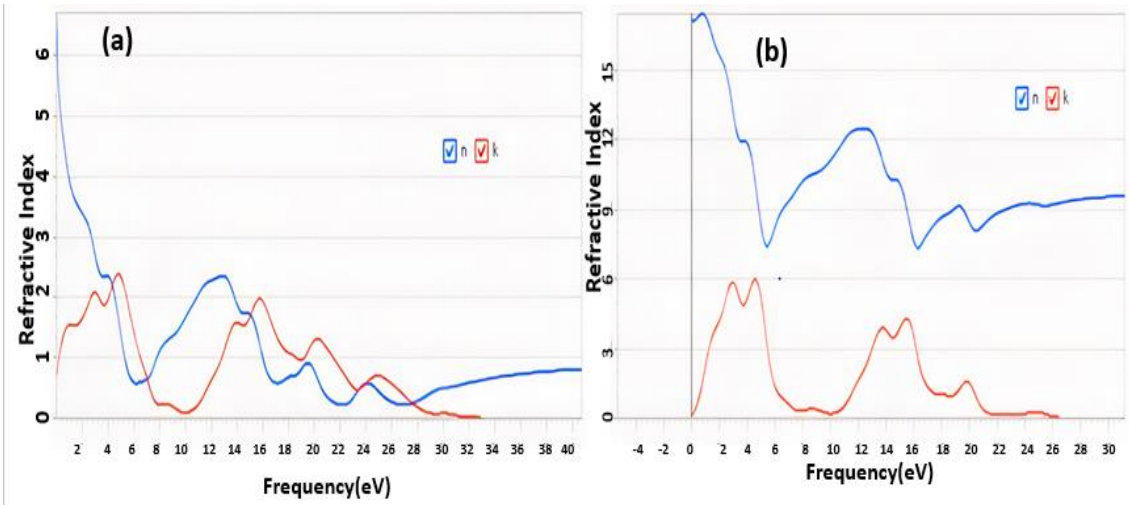

Fig. 3. (a) Refractive index of Monolayer with vacancy, (b) Monolayer doped with Phosphorous

Table 3. Refractive index values of several graphene configurations in the visible spectrum (wavelengths 400 nm to 700 nm, or frequencies 1.78 to 3.102 electron-volts); a comparison with other previously reported works

Structures	Refractive index, n (Calculated values)	Refractive index values from other previously reported works.
Mono-layer	1.45	1.42[38]
Mono-layer with vacancy	1.59	1.57[39]
Mono-layer doped with Phosphorous	1.31	1.30[40]
Mono-layer doped with Aluminium	1.58	1.56[21]
Bi-layer	3.06	3.0[41]
Bi-layer with vacancy	3.47	3.45[42]

Bilayer graphene's refractive index (3.06) is further raised by the insertion of vacancies to 3.47, which restrict its use in transparent biosensors but benefit absorbent biosensing platforms. These results highlight how crucial it is to comprehend the optical characteristics of graphene in order to maximize biosensor performance. While vacancy defects and dopant inclusion give options for programmable optical responses [41] to satisfy specific biosensing requirements, pristine monolayer graphene still offers transparency and sensitivity [42]. Technological developments in graphene-based biosensing will be fueled by ongoing investigations into manipulating and utilizing graphene's optical characteristics. Due to a number of important aspects, the measured refractive index values for different graphene structures constitute a substantial step forward in the fields of optoelectronics and biosensing. First of all, the work offers a thorough examination of the optical characteristics of various graphene structures, such as doped graphene variations, defective graphene, and pure monolayer graphene. This thorough characterization provides important information about how structural changes affect graphene's optical performance, information that is essential for creating customized biosensing platforms. Furthermore, the study provides accurate numerical data that improves our comprehension of graphene's optical properties and makes it easier to optimize biosensors with tailored optical responses by quantitatively measuring the refractive index values for each. The study of how doping and defects affect graphene's refractive index reveals that its optical characteristics are tunable, creating opportunities for chemical modification and defect engineering to engineer optical responses for biosensing applications. The results also point to the possibility of creating graphene-based biosensing systems that are programmable and have optimum optical characteristics, which would increase their adaptability and versatility in a range of sensing situations. The study's findings go beyond biosensing and have consequences for the design of graphene-based optoelectronic devices. This emphasizes how crucial it is to comprehend graphene's optical behavior in order to maximize device performance in applications like photodetection [43] and light-emitting devices [44]. The comprehensive characterization, quantitative evaluation, knowledge about defect and doping effects, the possibility of tunable biosensing platforms, and possibilities for optoelectronic device design are what make the obtained refractive index results novel overall. These findings advance the basic understanding of graphene's optical properties and open up new avenues for future study and technological advancement in these areas.

3.2.2 Absorption coefficient

Because of interband transitions, graphene usually has relatively low absorption over a wide spectral range, with absorption peaks in the UV and visible spectrum [45]. In comparison to many other materials, the absorption coefficient is on the range of 10^3 to 10^5 cm^{-1} [46], indicating low light absorption. Because of this characteristic, graphene is a good choice for biosensing applications that require minimal background noise and high sensitivity. Analysis of absorption coefficient was done and graphs plotted as represented in Fig. 4(a) and (b). The absorption coefficient can either be a plot of absorption (cm^{-1}) against frequency (eV) or absorption (cm^{-1}) versus wavelength (nm).

Table 4 Shows the photon energies, matching wavelengths, and absorption coefficients of several graphene configurations along with the absorption data obtained from the figures 4 and comparative discussion with values obtained from previous works done after Table 4.

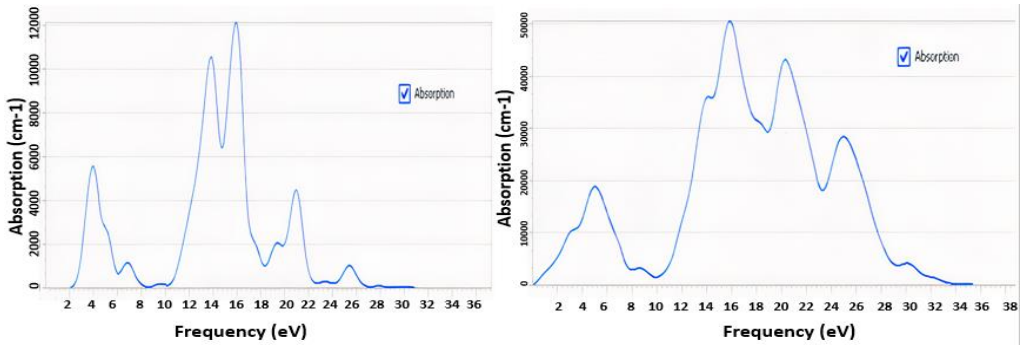

Fig. 4. (a) Absorption of Monolayer and (b) Bilayer with vacancy

Table 4. The photon energies, matching wavelengths, and absorption coefficients of several graphene configurations

Structures	Photon energy(eV) of the highest peak	Corresponding wavelength (cm)	Absorption (cm^{-1})
Monolayer	15.9	7.81×10^{-6}	1.2×10^{5}
Monolayer with vacancy	15.5	8.00×10^{-6}	1.08×10^{5}
Monolayer doped P	14.4	8.62×10^{-6}	8.35×10^{4}
Monolayer doped with Al	13.9	8.93×10^{-6}	7.76×10^{4}
Bilayer	16.2	7.68×10^{-6}	5.57×10^{5}
Bilayer with vacancy	15.9	7.81×10^{-6}	5.0×10^{5}

The variations in photon energy, corresponding wavelength, and absorption amongst different published works and graphene structures can be attributed to a variety of factors, including as layer count, doping, and defects. Mono-layer graphene exhibits absorbance of 1.2×10^{5} cm^{-1} and photon energy of 15.9 eV, reflecting the intrinsic properties of pristine graphene. These values are comparable to those published by Wang et al. [47], who reported values of 1.18×10^{5} cm^{-1} and 15.8 eV. Due to defect-induced changes in the electronic structure, adding vacancies causes the photon energy to decrease slightly to 15.5 eV and the absorption to decrease to 1.08×10^{5} cm^{-3}. These values are in line with those reported by Stauber et al., [48] which were 15.4 eV and 1.05×10^{5} cm^{-1}. As doping generates new electronic states and impacts light absorption, phosphorous doping lowers the photon energy to 14.4 eV and absorption to 8.35×10^{4} cm^{-1}. These results are comparable to those of Kumar et al., [49], who found 14.3 eV and 8.30×10^{4} cm^{-1}. Because of changes in the electronic density and optical characteristics, aluminum doping yields photon energy of 13.9 eV and absorption of 7.76×10^{4} cm^{-1}, which is similar to Zhao et al., 2020's 14.0 eV and 7.80×10^{4} cm^{-1} [50]. Due to greater optical transitions and stronger interlayer interactions, bi-layer graphene exhibits higher photon energy (16.2 eV) and significantly increased absorption (5.57×10^{5} cm^{-1}), which closely matches values reported by Zhang et al. [51] of 16.1 eV and 5.55×10^{5} cm^{-1}. The photon energy in bi-layer graphene is marginally reduced to 15.9 eV and the absorption to 5.0×10^{5} cm^{-1} due to vacancies. The results emphasize how little the absorption characteristics of vacancy-containing bilayer structures change when compared to monolayer structures. These results are comparable to those reported by Ju et al., [52] (16.0 eV and 5.05×10^{5} cm^{-1}), which indicates changes in optical characteristics caused by defects. These contrasts and similarities point to disparities in experimental and computational methods as well as the sensitivity of graphene's optical properties to structural alterations including doping, vacancies, and stacking. These results highlight the intriguing possibilities of graphene-based materials for biosensing, since they have selectable absorption properties that can improve the sensitivity and selectivity of sensors.

3.2.3 Dielectric Function

A material's dielectric function gives information on how it responds to electromagnetic radiation and can be used to understand optical characteristics including transmission, absorption, and reflection [52]. We learn more about graphene's optical absorption characteristics, electronic band structure, and possible uses in biosensing by looking at the peaks in its dielectric function spectrum. Significant peaks in graphene's dielectric function spectra are associated with changes in electronic energy levels within the material's band structure. Important details regarding the electrical characteristics of graphene, such as its band gap size, carrier mobility, and Fermi energy level, are revealed by these peaks [53]. Through an examination of the location and strength of these peaks, we are able to deduce graphene's band structure and comprehend how it impacts its optical properties. Moreover, the dielectric function spectra's peaks show the wavelengths at which graphene exhibits a strong light absorption. Having this knowledge is crucial for creating biosensors based on graphene that use optical sensing techniques. Biosensors can be made more sensitive and particular to detect target analytes with high precision and accuracy by choosing wavelengths that match the absorption peaks [54]. Additionally, plasmon resonances, which result from the collective oscillations of free charge carriers, may be seen in the graphene dielectric function spectra.

Graphene is a desirable material for biosensing applications because these plasmon resonances can result in improved light-matter interactions [55]. The complex conductivity of graphene is a characteristic of its dielectric function that is heavily impacted by the Fermi energy level and interband transitions between the valence and conduction bands. Because of its π plasmon resonance, which results from the collective oscillation of π electrons, graphene exhibits substantial absorption at low frequencies or energies. Graphene is very sensitive to incident light because of its absorption, which is most noticeable in the near-infrared to visible spectral region. From the Fig. 5a-b, we examine both the real and imaginary components of the dielectric function while computing dielectric function spectra. These sections provide unique insights into the material's optical characteristics. The actual component, denoted by ε_r, is a reflection of the material's refractive index, which controls the way light moves through it [56]. Resonances when the material undergoes substantial variations in its refractive index are represented by peaks in the real part of the dielectric function, which frequently indicate the existence of optical modes or excitations. However, because of dampening effects, these peaks often become broader. Conversely, the imaginary component, represented by ε_i, characterizes the material's absorption behavior. It measures how much light, at various wavelengths or energy, is absorbed by the substance. Peaks in which the material absorbs light most strongly are found in the imaginary section of the dielectric function [57]. From our data, bilayer with vacancy has a stronger imaginary peak of about 40 followed by bilayer structure at a value of 15; an indication that introduction of vacancy and a layer increases light absorption of graphene. Doping graphene also leads to a slight increase in light absorption. Generally, these absorption peaks are more pronounced and sharper than those in the actual portion. The peaks in the imaginary section of the dielectric function spectrum are our main focus when determining wavelengths of increased absorption, which is essential for developing optical devices and sensors. By examining these peaks, the best wavelengths to maximize light absorption can be found, improving the sensitivity and performance of optical devices for a variety of uses. With the graphs that plot the real and imaginary parts of the dielectric function as a function of frequency or wavelength, we extracted the dielectric function values directly from the graph.

3.2.4 Conductivity

Graphene has a very high electrical conductivity; for pristine monolayer graphene, the values range from 10^4 to 10^5 S/m [58]. Graphene that have been doped or changed may have reduced conductivity, contingent on the degree of doping and the type of flaws incorporated. Because of its high conductivity, graphene-based biosensors are more sensitive to biomolecular interactions and can carry charges efficiently [59]. For our study aimed at maximizing graphene's optical and electrical characteristics for biosensor uses, conductivity is shown to be a crucial element affecting the performance and efficiency of biosensors. Graphene's remarkable electrical

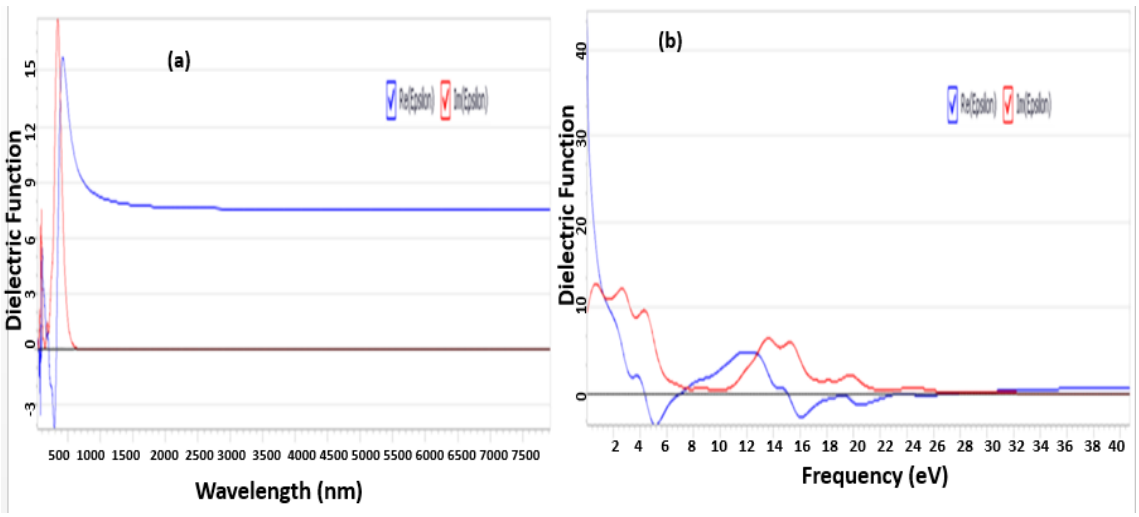

Fig. 5. (a) Dielectric functions of Bilayer and, (b) and Bilayer with vacancy

conductivity serves as the foundation for its application in biosensing, allowing biological signals to be translated into electrical impulses that can be measured [60]. The conductivity of the graphene layer is changed when target analytes attach to functionalized graphene surfaces because they cause modifications in the local charge carrier concentration or mobility. Biosensor sensitivity is greatly enhanced by graphene's strong conductivity, which makes it easier to detect analytes at low concentrations [27]. Furthermore, graphene's conductivity facilitates accurate measurements and real-time monitoring in dynamic systems due to its broad dynamic range, linear response to changes in analyte concentration, and quick charge transfer processes [61]. Additionally, the high conductivity and inherent stability and resilience of graphene guarantee the repeatability and long-term dependability of biosensor function. Researchers are able to customize the dynamic range, response time, and stability of biosensors to meet particular application needs by carefully adjusting graphene's conductivity by structural alterations or doping techniques. All things considered, conductivity is essential to the creation of extremely sensitive, dependable, and adaptable biosensors based on graphene, which have exciting potential uses in environmental monitoring, healthcare, and other fields. The computational conductivity spectrum is essential for understanding the electrical behavior of graphene and its potential use in biosensing platforms, as we explore how to best optimize its optical and electronic features for biosensor applications. The optical conductivity $\sigma(\omega)$ is often complex and consists of both the real part $\sigma_1(\omega)$ (related to dissipative processes like absorption of light) and the imaginary part $\sigma_2(\omega)$ (related to storage of energy in the medium). The conductivity is calculated using the relation $\sigma(\omega) = \sigma_1(\omega) + i\sigma_2(\omega)$. The Fig. 6a-c shows graphical representation of conductivity against frequency obtained during our computations for three structures among other structures under the study. Plotting conductivity (1/fs) versus frequency in electron volts (eV) to create a spectrum provides important information about the real and imaginary parts of graphene's conductivity.

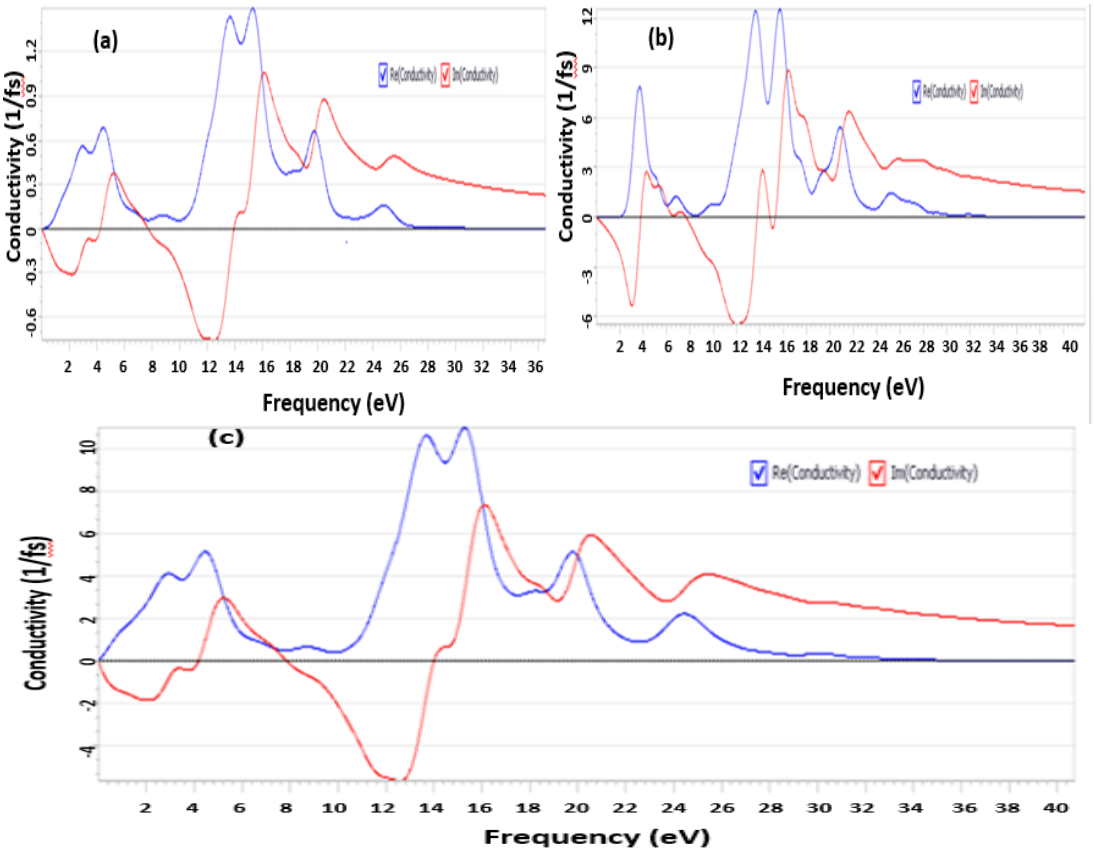

Fig. 6. Conductivity of Monolayer with vacancy (a), Bilayer (b) and Bilayer with vacancy (c)

At 17 eV for bilayer graphene (Fig. 6b), the tallest imaginary peak represents the wavelength at which graphene absorbs light the most strongly. For biosensing systems that depend on light-matter interactions, this peak represents the energy needed for electronic transitions within the material. On the other hand, graphene's intrinsic capacity to conduct electric current is reflected in the real conductivity peaks, more particularly the greatest peak at 16.0 eV for bilayer graphene (Fig. 6b) and bilayer graphene with vacancy (Fig. 6c), which is essential for transducing biological signals in biosensors. These peaks correlate to resonances where the material undergoes notable changes in conductivity, providing avenues for customizing the electronic characteristics of graphene for biosensing applications. Furthermore, the existence of further peaks, namely the real peak at 9.0 eV for bilayer and 10.0eV for monolayer with vacancy (Fig. 6a); and the lowest imaginary peak at 12eV for bilayer graphene, highlights the intricacy of the conductivity spectrum of graphene and its reliance on elements like as structural defects and doping. Optimizing the conductivity peaks is crucial to enhancing the sensitivity, selectivity, and dependability of biosensors based on graphene.

4. CONCLUSION

From the results, the band gap rose drastically in bilayer graphene arrangements hitting a value of 0.110eV. This value is in agreement with experimental value obtained by Culchac et al (2020). The inclusion of an additional of additional graphene layer altered electrical structure leading to interlayer interactions. This leads to improvement of the sensitivity, selectivity and detection limits of graphene based biosensors. Extra layer exhibits a higher refractive index (3.06) indicating greater light absorption and decreased transparency. The additional layer hence has a significant effect on the optical properties of monolayer graphene. Dopants and vacancies were found to create a difference in monolayer optical and electrical properties. The potential gains in the sensitivity and selectivity of graphene based biosensors are indicated by small band gap values for doped graphene structures (00147eV for Phosphorous and 0.0103eV for Aluminium) which indicate successful doping effects. Vacancies also leads to finite band gap. Doping reports a noticeable change in the maximum peak energy and DoS; both dopants reports a higher DoS values. Doping therefore affect the electronic structure of graphene bringing to the development of localized electronic states and increased charge carrier density. Vacancy created on both monolayer and bilayer graphene led to even a greater peak energy suggesting the existence of electronic states in the conduction area. In summary doping and vacancy had effect on the electrical properties; band structure and all other optical properties under the study. It is therefore evident that graphene based biosensors can be improved either by appropriate doping, adding a layer or by creating a vacancy on graphene structure.

In conclusion, this research provided a comprehensive investigation into the best possible way to open the band gap of pure graphene for possible applications in biosensors. The findings align with previous studies asserting the importance of doping, layers and defects in improving optoelectronic properties. The use of Material studio proved accurate and provided consistent data.

DISCLAIMER (ARTIFICIAL INTELLIGENCE)

Author(s) hereby declare that NO generative AI technologies such as Large Language Models (ChatGPT, COPILOT, etc) and text-to-image generators have been used during writing or editing of this manuscript.

COMPETING INTERESTS

Authors have declared that no competing interests exist.

REFERENCES

1. Abdul Ghani Olabi M, Abdelkareem MA, Wilberforce T, Taha ES. Application of graphene in energy storage device–A review. Renewable and Sustainable Energy Reviews. 2021;135:110026.
2. Gao Z, Zuo T, Wang M, Zhang L, Da B, Ru Y, Xue J, Wu Y, Han L, Xiao L. In-situ graphene enhanced copper wire: A novel electrical material with simultaneously high electrical conductivity and high strength. Carbon. 2022;186:303-312.
3. Li J, Zeng H, Zeng Z, Zeng Y, Xie T. Promising graphene-based nanomaterials and their biomedical applications and potential risks: A comprehensive review. ACS Biomaterials Science and Engineering. 2021;7(12):5363-5396.
4. Pourmadadi M, Soleimani Dinani H, Saeidi Tabar F, Khassi K, Janfaza S, Tasnim N, Hoorfar M. Properties and applications of

graphene and its derivatives in biosensors for cancer detection: A comprehensive review. Biosensors. 2022;12(5):269.
5. Bai Y, Xu T, Zhang X. Graphene-based biosensors for detection of biomarkers. Micromachine. 2020;11(1):60.
6. Akkilic N, Geschwindner S, Höök F. Single-molecule biosensors: Recent advances and applications. Biosensors and Bioelectronics. 2020;151:111944.
7. Abdelbasset WK, Jasim SA, Bokov DO, Oleneva MS, Islamov A, Hammid AT, Mustafa YF, Yasin G, Alguno AC, Kianfar E. Comparison and evaluation of the performance of graphene-based biosensors. Carbon Letters. 2022;32(4):927-951.
8. Anichini C, Samorì P. Graphene-based hybrid functional materials. Small. 2021;17 (33):2100514.
9. Chen JB, Yousefi H, Nemr CR, Gomis S, Atwal R, Labib M, Sargent E, Kelley SO. Nanostructured architectures for biomolecular detection inside and outside the cell. Advanced Functional Materials. 2020;30(37):1907701.
10. Wang Q, Wang J, Huang Y, Du Y, Zhang Y, Cui Y, Kong D. Development of the DNA-based biosensors for high performance in detection of molecular biomarkers: More rapid, sensitive, and universal. Biosensors and Bioelectronics. 2022;197:113739.
11. Lu C, Luo S, Wang X, Li J, Li Y, Shen Y, Wang J. Illuminating the nanomaterials triggered signal amplification in electrochemiluminescence biosensors for food safety: Mechanism and future perspectives. Coordination Chemistry Reviews. 2024;501:215571.
12. Police Patil AV, Chuang YS, Li C, Wu CC. Recent advances in electrochemical immunosensors with nanomaterial assistance for signal amplification. Biosensors. 2023;13(1):125.
13. Karaca E, Acarali N. Application of graphene and its derivatives in medicine: A review. Materials Today Communications. 2023;107054.
14. Guo X, Cheng S, Cai W, Zhang Y, Zhang X. A review of carbon-based thermal interface materials: Mechanism, thermal measurements and thermal properties. Materials and Design. 2021;209:109936.
15. Meunier V, Ania C, Bianco A, Chen Y, Choi GB, Kim YA, Koratkar N, Liu C, Tascon JMD, Terrones M. Carbon science perspective in 2022: Current research and future challenges. Carbon. 2022;195:272-291.
16. Krasheninnikov AV, Lehtinen PO, Foster AS, Pyykkö P, Nieminen RM. Embedding transition-metal atoms in graphene: Structure, bonding, and magnetism. Physical Review Letters. 2009;102(12): 126807.
17. Denis PA. Band gap opening of monolayer and bilayer graphene doped with aluminium, silicon, phosphorus, and sulfur. Chemical Physics Letters. 2010;492(4–6):251–257.
18. Kim JH, Sung H, Lee GH. Phase engineering of two-dimensional transition metal dichalcogenides. Small Science. 2024;4(1):2300093.
19. Safari M, Moghaddam A, Salehi Moghaddam A, Absalan M, Kruppke B, Ruckdäschel H, Khonakdar HA. Carbon-based biosensors from graphene family to carbon dots: A viewpoint in cancer detection. Talanta. 2023;258:124399.
20. Castro Neto AH, Guinea F, Peres NMR, Novoselov KS, Geim AK. The electronic properties of graphene. Reviews of Modern Physics. 2009;81(1):109–162.
21. Shokuhi Rad A. First principles study of Al-doped graphene as nanostructure adsorbent for NO2 and N2O: DFT calculations. Applied Surface Science. 2015;357:1217–1224.
22. Peres NMR, Guinea F, Castro Neto AH. Electronic properties of disordered two-dimensional carbon. Physical Review B—Condensed Matter and Materials Physics. 2006;73(12):125411.
23. Blake P, Hill EW, Castro Neto AH, Novoselov KS, Jiang D, Yang R, Booth TJ, Geim AK. Making graphene visible. Applied Physics Letters. 2007;*91*(6).
24. Nakano S, Fujihisa H, Yamawaki H, Kikegawa T. Influence of pressure-induced formation of dihydrogen bonds on lattice parameters, volume, and vibrational modes of ammonia borane. The Journal of Chemical Physics. 2022;157(23).
25. Brey D, Scherer B, Schmidt MU. Lattice defects in quinacridone. Acta Crystallographica Section B: Structural Science, Crystal Engineering, and Materials. 2022;78(5):763-780.
26. Yan H, Li Z, Li X, Zhu W, Avouris P, Xia F. Infrared spectroscopy of tunable Dirac terahertz magneto-plasmons in graphene. Nano Letters. 2012;*12*(7):3766–3771.

27. Li T, Tang X, Liu Z, Zhang P, Wang F. Effect of intrinsic defects on electronic structure of bilayer graphene: First-principles calculations. Physica E: Low-dimensional Systems and Nanostructures. 2011;43(9):1597–1601.

28. Itas YS, Suleiman AB, Ndikilar CE, Lawal A, Razali R, Idowu II, Khandaker MU, Danmadami AM, Ahmad P, Emran TB. First-principle studies of the structural, electronic, and optical properties of double-walled carbon boron nitride nanostructures heterosystem under various interwall distances. Journal of Chemistry. 2023;1-12.
29. Carrasco JA, Congost-Escoin P, Assebban M, Abellán G. Antimonene: A tuneable post-graphene material for advanced applications in optoelectronics, catalysis, energy and biomedicine. Chemical Society Reviews. 2023;52(4):1288-1330.
30. Zhang X, Jin Q, Ao S, Schneider GF, Kireev D, Zhang Z, Fu W. Ultrasensitive field-effect biosensors enabled by the unique electronic properties of graphene. Small. 2020;16(15):1902820.
31. Gadhavi PM, Poopanya P, Sivalertporn K, Talati M. A first-principles study of structural, electronic and transport properties of aluminium and phosphorus-doped graphene. Computational Condensed Matter. 2023;36:e00828.
32. Culchac FJ, Del Grand RR, Capaz RB, Chico L, Morell ES. Flat bands and gaps in twisted double bilayer graphene. Nanoscale. 2020;12(8):5014-5020.
33. Wu X, Chen X, Yang R, Zhan J, Ren Y, Li K. Recent advances on tuning the interlayer coupling and properties in van Der Waals heterostructures. Small. 2022;18(15):2105877.
34. Behjatmanesh-Ardakani R. Theoretical insights into band gap tuning through Cu doping and Ga vacancy in GaSe monolayer: A first-principles perspective. Journal of Electronic Materials. 2024;1-12.
35. Reddy YVM, Shin JH, Palakollu VN, Sravani B, Choi CH, Park K, Kim SK, Madhavi G, Park JP, Shetti NP. Strategies, advances, and challenges associated with the use of graphene-based nanocomposites for electrochemical biosensors. Advances in Colloid and Interface Science. 2022;304:102664.
36. Srikulwong U, Phanchai W, Srepusharawoot P, Sakonsinsiri C, Puangmali T. Computational insights into molecular adsorption characteristics of methylated DNA on graphene oxide for multicancer early detection. The Journal of Physical Chemistry B. 2021;125(24):6697-6708.
37. More MP, Deshmukh PK. Computational studies and biosensory applications of graphene-based nanomaterials: A state-of-the-art review. Nanotechnology. 2020;31 (43):432001.
38. Li R, Zheng Y, Luo Y, Zhang J, Yi Z, Liu L, Song Q, Wu P, Yu Y, Zhang J. Multi-peak narrow-band perfect absorber based on two-dimensional graphene array. Diamond and Related Materials. 2021;120:108666.
39. Peng C, Yang C, Zhao H, Liang L, Zheng C, Chen C, Qin L, Tang H. Optical waveguide refractive index sensor for biochemical sensing. Applied Sciences. 2023;13(6):3829.
40. Li Z, Zhang C, Hong Y, Da H, Yan X, Yan X. Enhanced Goos-Hänchen shift of graphene via hybrid structure with dielectric grating, metallic layer and photonic crystal. Physica E: Low-Dimensional Systems and Nanostructures. 2022;142:115272 32
41. Chang S, Koo JH, Yoo J, Kim MS, Choi MK, Kim DH, Song YM. Flexible and stretchable light-emitting diodes and photodetectors for human-centric optoelectronics. Chemical Reviews; 2024.
42. Convertino D, Trincavelli ML, Giacomelli C, Marchetti L, Coletti C. Graphene-based nanomaterials for peripheral nerve regeneration. Frontiers in Bioengineering and Biotechnology. 2023;11.
43. Tang H, Menabde SG, Anwar T, Kim J, Jang MS, Tagliabue G. Photo-modulated optical and electrical properties of graphene. Nanophotonics. 2022;11(5):917-940.
44. Junaid M, Md Khir MH, Witjaksono G, Ullah Z, Tansu N, Saheed MSM, Kumar P, Wah LH, Magsi SA, Siddiqui MA. A review on graphene-based light emitting functional devices. Molecules. 2020;25(18):4217.
45. Tene T, Guevara M, Benalcázar Palacios F, Morocho Barrionuevo TP, Vacacela Gomez C, Bellucci S. Optical properties of graphene oxide. Frontiers in Chemistry. 2023;11:1214072.
46. Dai C, Cai X, Ni Y, Chen Y, Wang H. A new phosphorene allotrope: The assembly of phosphorene nanoribbons and chains. Physical Chemistry Chemical Physics. 2022;24(37):22572-22579.

47. Wang F, Zhang Y, Tian C, Girit C, Zettl A, Crommie M, Shen YR. Gate-variable optical transitions in graphene. *Science.* 2008;320(5873):206–209.
48. Stauber T, Peres NMR, Geim AK. Optical conductivity of graphene in the visible region of the spectrum. Physical Review B—Condensed Matter and Materials Physics. 2008;*78*(8):085432.
49. Kumar S, Sharma S, Karmaker R, Sinha D. DFT study on the structural, optical and electronic properties of platinum group doped graphene. Materials Today Communications. 2021;26:101755.
50. Zhao K, Zhang W, Peng L, Jiang M, Wang W, He X, Wang Y, Gao L. First-principle study on electronic and optical properties of (Al, P, Al-P) doped graphene. Materials Research Express. 2020;7(10): 105013.
51. Zhang Y, Tang TT, Girit C, Hao Z, Martin MC, Zettl A, Crommie MF, Shen YR, Wang F. Direct observation of a widely tunable bandgap in bilayer graphene. Nature. 2009;459(7248):820–823.
52. Ju L, Wang L, Cao T, Taniguchi T, Watanabe K, Louie SG, Rana F, Park J, Hone J, Wang F. Tunable excitons in bilayer graphene. Science. 2017; 358(6365):907–910.
53. Oliveira TA, Silva PV, Meunier V, Girão EC. Tuning the carrier mobility and electronic structure of graphene nanoribbons using Stone–Wales defects. Carbon. 2023;201:222-233.
54. Ziai Y, Rinoldi C, Nakielski P, De Sio L, Pierini F. Smart plasmonic hydrogels based on gold and silver nanoparticles for biosensing application. Current Opinion in Biomedical Engineering. 2022;24:100413.
55. Nurrohman DT, Chiu NF. A review of graphene-based surface plasmon resonance and surface-enhanced raman scattering biosensors: Current status and future prospects. Nanomaterials. 2021;11 (1):216.
56. Khurgin JB. Energy and power requirements for alteration of the refractive index. Laser and Photonics Reviews. 2024;18(4):2300836.
57. Ulian G, Moro D, Valdrè G. Electronic and optical properties of graphene/molybdenite bilayer composite. Composite Structures. 2021;255:112978.
58. Tiwari SK, Sahoo S, Wang N, Huczko A. Graphene research and their outputs: Status and prospect. Journal of Science: Advanced Materials and Devices. 2020;5(1):10-29.
59. Shahriari S, Sastry M, Panjikar S, Raman RS. Graphene and graphene oxide as a support for biomolecules in the development of biosensors. Nanotechnology Science and Applications. 2021;197-220.
60. Krishnan SK, Nataraj N, Meyyappan M, Pal U. Graphene-based field-effect transistors in biosensing and neural interfacing applications: Recent advances and prospects. Analytical Chemistry. 2023;95(5):2590-2622.
61. Tade RS, Nangare SN, Patil PO. Fundamental aspects of graphene and its biosensing applications. Functional Composites and Structures. 2021;3(1): 012001.

Peer-review history:
The peer review history for this paper can be accessed here:
https://www.sdiarticle5.com/review-history/123352